Journal of Clinical and Translational Hepatology **2024** vol. 12(11) | 917–929
DOI: 10.14218/JCTH.2024.00135

Original Article

GPX4 Promoter Hypermethylation Induced by Ischemia/Reperfusion Injury Regulates Hepatocytic Ferroptosis

Chen Bai[#], Peilun Xiao[#], Yuting Chen, Fangfang Chu, Yue Jiao, Jiaqi Fan, Yuexia Zhang, Jiao Liu, Jiying Jiang[*] and Shuna Yu[*]

Department of Anatomy, School of Basic Medical Sciences, Shandong Second Medical University, Weifang, Shandong, China

Received: April 14, 2024 | **Revised:** September 11, 2024 | **Accepted:** September 29, 2024 | **Published online:** October 18, 2024

Abstract

Background and Aims: Glutathione peroxidase 4 (GPX4) is a key factor in ferroptosis, which is involved in ischemia-reperfusion injury. However, little is known about its role in hepatic ischemia-reperfusion injury (HIRI). This study aimed to investigate the role of GPX4 methylation in ferroptosis during HIRI. ***Methods:*** For the *in vitro* experiments, an oxygen and glucose deprivation cell model was established. For the *in vivo* experiments, an ischemia-reperfusion model was created by subjecting mice to simulated HIRI. Ferroptosis occurrence, *GPX4* promoter methylation, and global methylation levels were then assessed. ***Results:*** Ferroptosis was observed in oxygen and glucose deprivation, characterized by a significant decrease in cellular viability ($P < 0.05$), an increase in lipid peroxidation ($P < 0.01$), iron overload ($P < 0.05$), and down-regulation of GPX4 ($P < 0.05$). This ferroptosis was exacerbated by GPX4 knockdown ($P < 0.01$) and mitigated by exogenous glutathione ($P < 0.01$). Similarly, ferroptosis was evident in mice subjected to HIRI, with a down-regulation of GPX4 mRNA and protein expression (all $P < 0.01$), and an upregulation of acyl-CoA synthetase long-chain family member 4 mRNA and protein (all $P < 0.01$), as well as prostaglandin-endoperoxide synthase 2 mRNA and protein expression (all $P < 0.05$). Methylation levels increased, evidenced by upregulation of DNA methylation transferase expression ($P < 0.05$) and down-regulation of Ten-eleven translocation family demethylases ($P < 0.01$), along with an upregulation of *GPX4* promoter methylation. ***Conclusions:*** Ferroptosis may be the primary mode of cell death in hepatocytes following ischemia-reperfusion injury. The methylation of the *GPX4* promoter and elevated levels of global hepatic methylation are involved in the regulation of ferroptosis.

Citation of this article: Bai C, Xiao P, Chen Y, Chu F, Jiao Y, Fan J, *et al*. GPX4 Promoter Hypermethylation Induced by Ischemia/Reperfusion Injury Regulates Hepatocytic Ferroptosis. J Clin Transl Hepatol 2024;12(11):917–929. doi: 10.14218/JCTH.2024.00135.

Keywords: Glutathione peroxidase 4; Promoter; Methylation; Oxygen and glucose deprivation cell model; Hepatic ischemia-reperfusion injury; Ferroptosis; Lipid peroxidation; Iron overload.

[#]Contributed equally to this work.

[*]**Correspondence to:** Jiying Jiang and Shuna Yu, Department of Anatomy, School of Basic Medical Sciences, Shandong Second Medical University, Weifang, Shandong 261053, China. ORCID: https://orcid.org/0009-0004-2238-8234 (JJ) and https://orcid.org/0000-0001-5537-995X (SY). Tel: +86-536-8462049, E-mail: jiangjiying2002@163.com (JJ) and yushn@sdsmu.edu.cn (SY).

Introduction

Hepatic ischemia-reperfusion injury (HIRI) is one of the main causes of poor outcomes after hepatic surgery,[1] yet little is known about its molecular mechanism.[2] A potential link has been proposed between ferroptosis and ischemia-reperfusion injury (IRI), as IRI is typically accompanied by ferroptosis-related phenotypes such as increased lipid peroxidation and elevated iron levels.[3,4] In addition, ferroptosis is associated with altered expression of proteins, such as upregulation of acyl-CoA synthetase long-chain family member 4 (ACSL4) and prostaglandin-endoperoxide synthase 2 (PTGS2), as well as downregulation of glutathione peroxidase 4 (GPX4). Previous studies have shown that administration of Ferrostatin-1 (Fer-1, a specific ferroptosis inhibitor), iron chelators, and antioxidants can mitigate ischemia-reperfusion (I/R)-induced cardiomyocyte injury,[3] while a high-iron diet can exacerbate liver injury.[5] These findings lead us to investigate the driving factors of ferroptosis during the onset of HIRI.

During ferroptosis, ACSL4 catalyzes polyunsaturated fatty acids, particularly arachidonic acid, into their CoA derivatives, enhancing lipid peroxidation.[6,7] Various studies have demonstrated that changes in ACSL4 are essential for triggering ferroptosis, with its expression levels determining the sensitivity of cells to ferroptosis. [7–9] Overexpression of ACSL4 increases cellular sensitivity to ferroptosis and promotes the process, while inhibition or knockdown of ACSL4 suppresses ferroptosis[6] establishing it as a key initiator in this cell death pathway. As a marker of ferroptosis in various cell types,[10,11] PTGS2 facilitates the conversion of arachidonic acid to prostaglandins. Research from the Stockwell laboratory has identified PTGS2 as a downstream marker of ferroptosis, showing significant upregulation during this process.[12] Bioinformatics analysis also indicates that PTGS2 is a central gene involved in ferroptosis.[13] PTGS2 expression has been closely associated with ferroptosis in various diseases. For example, PTGS2 levels are significantly elevated during ferroptosis induced by hormone-related femoral head necrosis.[11] In liver ferroptosis studies, the AhR-STAT3-Hmox1/PTGS2 signaling pathway has been found to improve the liver microenvironment by inhibiting ferroptosis.[14] Additionally, research has shown that upregulation of PTGS2 and ACSL4 contributes to atherosclerosis-associated ferroptosis.[13] GPX4, a key regulatory factor of ferroptosis, uses glutathione (GSH) to detoxify lipid peroxidation.[15] In *GPX4* knockout mice, massive hepatocyte degeneration and death were observed,[16] while cells with *GPX4* overexpression exhibited increased tolerance to ferroptosis.[17] Similarly, GPX4 deficiency induced ferroptosis in renal

tubular epithelial cells, neuronal cells, endothelial cells, and T cells.[18,19] Furthermore, *GPX4* expression was downregulated in non-alcoholic fatty liver disease and drug-induced liver injury, while exogenous GSH could restore hepatocyte structure and function.[4] These markers are therefore used to study the ferroptosis mechanisms underlying HIRI.

DNA methylation is a common epigenetic modification involved in various pathological processes (e.g. IRI),[20] with CpG dinucleotide being the major site on promoters.[21] This process relies on the dynamic regulation of DNA methyltransferases (DNMTs) and the ten-eleven translocation (TET) family of proteins.[22] DNMTs transfer a methyl group from S-adenosyl-L-methionine to adenine or cytosine bases within DNA sequences.[23] TET proteins catalyze the oxidation of 5-methylcytosine (5mC) in CpG, producing 5-hydroxymethylcytosine (5hmC), which regulates DNA demethylation.[24] Although the role of DNA methylation regulation in HIRI has not been reported, abnormal DNA methylation has been observed in liver diseases such as alcoholic fatty liver, viral hepatitis, intermittent hypoxia-induced liver injury, hepatic fibrosis, and hepatocellular carcinoma.[5,20,25] During IRI, there is a general increase in cellular methylation, along with alterations in demethylase and methylase levels.[26] Furthermore, inhibiting DNA methylation has been shown to alleviate IRI and improve cellular function.[27] Based on this, we hypothesize that altered methylation of the *GPX4* promoter may be associated with ferroptosis in the pathogenesis of HIRI. To verify this hypothesis, we established a mouse HIRI model and an oxygen and glucose deprivation (OGD)-induced alpha mouse liver 12 (AML12) cell injury model, and determined ferroptosis-related factors and *GPX4* promoter methylation.

Methods

Chemicals and reagents

Fer-1 (HYG-100579), Benzyloxycarbonyl-Val-Ala-Asp (OMe)-fluoromethylketone (Z-VAD, HY-16658B), Necrostatin-1 (Nec-1, HY-15760), and 5-Azacytidine (5-AZA, HY-A0004) were purchased from MedChemExpress LLC (NJ, USA). Rabbit polyclonal antibody, including anti-GAPDH (Cat. no: 60004-1-Ig), was purchased from ProteinTech. Anti-DNMT3a (Cat. no: ab188470), anti-TET2 (Cat. no: ab213369), anti-GPX4 (Cat. no: ab125066), and anti-ACSL4 (Cat. no: ab155282) were purchased from Abcam. Anti-PTGS2 (BSM-52502R) was purchased from Bioss Biotechnology (Beijing, China). FITC-labeled goat anti-rabbit IgG (Cat. no: A0562) was purchased from Beyotime (Beijing, China). DAB color developing solution (Cat. no: PV-6001) was purchased from ZSGB-BIO (Beijing, China). Mounting medium with antifading (with DAPI, Cat. no: S2110) and the GPX Activity Assay Kit (Cat. no: BC1195) were purchased from Solarbio (Beijing, China). Alanine aminotransferase (ALT) Assay Kit (C009-2-1) and reduced GSH Assay Kit (A006-2-1) were purchased from Jiancheng Bioengineering Institute (Nanjing, China). The ReverTra Ace qPCR RT Kit (FSQ-101) was provided by Toyobo (Osaka, Japan). The cell counting kit-8 (CCK8, Cat. no: CK058) was purchased from Seven Sea Futai Biotechnology (Shanghai, China). The shGPX4 plasmid was designed by WZ Biosciences (Jinan, China). Lipofectamine 2000 (Cat. no: 1168-019) was obtained from Invitrogen (CA, USA). The fluorescence probes C11 BODIPY 581/591 (Cat. no: MX5211) and FerroOrange (Cat. no: MX4559) were obtained from Maokang Biotechnology (Shanghai, China). The DNA extraction kit (YDP304-03) and methylation-specific PCR kit (Cat. no: 4992447) were purchased from TIANGEN Biotech (Beijing, China). The EZ DNA Methylation-Gold kit (Cat. no: D5007) was purchased from Zymo research (CA, USA). Methylation-specific PCR kit (Cat. no: HY-A0004) was obtained from MedChemExpress (New Jersey, USA). The methylation (Cat. no: D5325) and hydroxymethylation ELISA kits (Cat. no: D5426) were from A&D Technology Corporation (Beijing, China).

Cell culture and grouping

An OGD model was designed in this section to mimic HIRI conditions *in vitro*. AML12 cells in the logarithmic growth phase were resuspended in 0.25% trypsin, inoculated into well plates, and divided into a control group and an OGD group as follows. The cells in the control group were cultured using DME/F-12 medium supplemented with 10% fetal bovine serum (FBS) in a cell culture incubator at 37°C in 95% air. To mimic a cell injury model, the OGD group was set up,[28] in which the cells were cultured in serum-free DME/F-12 medium in a triple air incubator at 37°C in 95% nitrogen for 12 h, followed by replacement with medium supplemented with 10% FBS in a normoxic incubator for 4 h. To explore the effects of other drugs in the OGD model, AML12 cell suspension was inoculated onto a 96-well plate and cultured overnight in medium containing 10% FBS under normoxic conditions. Upon reaching 80% confluence, drug pretreatment was performed, followed by the preparation of the OGD model. The cells were treated with drugs, including Fer-1 (2 μM), Z-VAD (25 μM), and Nec-1 (50 μM) for 2 h to investigate the predominant mode of cell death. The cells were then treated with GSH (100 μM) for 2 h to assess the impact of GPX4,[29–31] followed by treatment with 5-AZA (25 μM) for 72 h to explore the potential methylation effects on GPX4.

CCK8 assay

The CCK8 colorimetric kit was used to detect cell viability in each group. In brief, 100 μL of solution was added to each well and incubated in a cell culture incubator for 2 h.[32] The optical density (OD) value at 450 nm was measured using a microplate reader, and cell viability was calculated according to the manufacturer's instructions.

Animals and modeling process

One hundred and eight healthy male C57BL/6 mice (six to eight weeks old, weighing 22–25 g) that were specific pathogen free were obtained from Pengyue Experimental Animal Center (Jinan, China). The mice were placed in laboratory cages and given free access to food and water. After one week of adaptation in a controlled environment (constant temperature, humidity, and a 12 h light/dark cycle), the animals were randomly divided into the following groups: I/R group (n = 18), I/R+Fer-1 group (n = 18), I/R+Z-VAD group (n = 18), I/R+Nec-1 group (n = 18), and sham operation group (n = 18). The HIRI model was performed according to our previous description.[33,34] Briefly, the animals in the I/R group were anesthetized with 1% sodium pentobarbital (40 mg/kg) via intraperitoneal injection. The left and middle branches of the hepatic pedicle were clamped with non-invasive arterial clips for 45 m, followed by reperfusion for 6 h, 12 h, or 24 h. The three treated groups received intraperitoneal injections of 0.5 mg/kg of Fer-1, 1.0 mg/kg of Z-VAD, and 3 mg/kg of Nec-1, respectively, 30 m before HIRI modeling.[29] The mice in the sham group underwent the same procedure as the I/R group, except that the hepatic pedicle branches were not occluded. After reperfusion, 72 mice from the three groups were anesthetized intraperitoneally with 1% sodium pentobarbital, and blood samples were collected from each mouse by retro-orbital bleeding. The blood samples were stored at room temperature for 40 m, followed by centrifugation at 3,000 rpm/m

for 10 m. The upper serum layer was collected and stored at −80°C. The left lobe of the liver was clipped and stored at −80°C for DNA, mRNA, and protein extraction. The remaining 36 mice were anesthetized and perfused with 4% paraformaldehyde for the preparation of paraffin-embedded or frozen sections, which were used for immunohistochemistry (IHC) and immunofluorescence (IF) staining.

Animal experiments were conducted in accordance with the guidelines for the use of experimental animals, and all procedures were approved by the Animal Ethics Committee of Shandong Second Medical University (No. 2020SDL187). The operative mortality rate was less than 3%.

Serum ALT measurement

Serum ALT was detected using Wright's microplate method, and the OD value at 510 nm was measured using a microplate reader (Thermo, Shanghai, China) as previously described.[35,36] The ALT value (U/L) was calculated after at least three tests.

GSH and GPX4 measurement

The GSH concentration was measured following the method described in a previous study.[37] The OD values were measured at 405 nm using a microplate reader. The concentration of GPX4 was measured using a commercial kit. Briefly, hepatic tissues (50 mg) were homogenized on ice, transferred to 1.5 mL Eppendorf tubes, and reagents were added according to the kit instructions for 15 m. Finally, the OD value was determined at 412 nm using a microplate reader. All measurements were performed in triplicate.

Fluorescence probe staining

C11 BODIPY 581/591[38] and FerroOrange are sensitive fluorescent probes for cellular lipid peroxides and ferrous ions, respectively. The control group and OGD model were constructed according to the methods outlined above. The culture medium from both groups was discarded, and the cells were rinsed with pre-cooled PBS three times. Serum-free medium containing C11 BODIPY 581/591 (50 μM) or FerroOrange (1 μM) was added and incubated at 37°C in the dark for 30 m. After routine washing and DAPI staining, the plates were observed under an inverted microscope.[39] C11 BODIPY 581/591 staining was observed in the FITC 488 nm and PI 565 nm channels. FerroOrange staining was observed in the PI channel, and images were captured and analyzed.

To further clarify the respective OD changes of the two fluorescent dyes induced by OGD modeling, AML12 cells were inoculated into light-avoiding transparent-bottom 96-well plates, incubated, stained, and washed as before. At the end of incubation, 100 μL of pre-cooled PBS was added to each well. The OD values were collected at 510 nm and 591 nm, respectively. The $OD_{591nm/510nm}$ ratio was used to indicate the degree of lipid peroxidation, while the OD value measured at 565 nm represented the ferrous ion content in the cells.

IHC staining

Paraffin sections were routinely dewaxed, hydrated, and underwent antigen retrieval. Anti-DNMT3a (1:200) and anti-TET2 (1:200) were added and incubated at 4°C overnight. After washing with PBS three times, the sections were incubated with secondary antibodies for 1 h. DAB color developing solution (1:20) was then applied, followed by hematoxylin staining, and the sections were evaluated by pathologists.[40]

IF staining

Frozen sections were blocked for endogenous peroxidase activity with 3% H_2O_2 for 10 m, then rinsed with PBS for 5 m. The sections were blocked with normal goat serum for 10 m and incubated overnight at 4°C with anti-GPX4 (1:500), anti-ACSL4 (1:500), and anti-PTGS2 (1:500). After washing with PBS for 5 m, the sections were incubated for 2 h with FITC-labeled goat anti-rabbit IgG at 37°C in the dark. The sections were then rinsed with PBS for 5 m, sealed with antifade mounting medium (with DAPI), and evaluated by pathologists using a fluorescence microscope (Olympus FV500, Olympus Corporation).[40]

GPX4 knockdown

The shGPX4 plasmid was used to knock down *GPX4*. The sequence of the shGPX4 plasmid is listed in Supplementary Table 1. AML12 cells were inoculated onto a 96-well plate and cultured overnight. Transfection was performed using Lipofectamine 2000 according to previously described methods.[41]

Real-time polymerase chain reaction (RT-qPCR)

Total mRNA was extracted from liver tissue or AML12 cells using a Trizol reagent. cDNA was synthesized using a ReverTra Ace qPCR RT Kit. The system components and procedures are described in Supplementary Table 2. PCR was performed using SYBR Green with specific primers purchased from Jinweizhi (Tianjin, China). The conditions were as follows: pre-denaturation at 95°C for 3 m, annealing at 60°C for 45 s, for a total of 35 cycles. The primer sequences are listed in Supplementary Table 3. Target gene expression was calculated using the $2^{-\Delta\Delta Ct}$ method, as previously described.[42]

Western blotting analysis

Total protein was extracted from liver tissue homogenized in RIPA lysate on ice with a protease inhibitor. Protein concentration was determined using the bicinchoninic acid assay.[35] Next, proteins were subjected to SDS-PAGE gel electrophoresis and then transferred to PVDF membranes. The membranes were blocked with skimmed milk and incubated overnight at 4°C with rabbit polyclonal antibodies: anti-GAPDH (1:1,000), anti-ACSL4 (1:2,000), anti-GPX4 (1:1,000), anti-TET2 (1:1,000), anti-PTGS2 (1:1,500), and anti-DNMT3a (1:1,000). The membranes were then incubated with horseradish peroxidase-conjugated secondary antibodies at room temperature for 1 h, followed by the addition of ECL developing solution. GAPDH was used as the internal reference protein. Finally, the images were analyzed using ImageJ 1.8.0 software (National Institutes of Health).

GPX4 promoter methylation sequencing

CpG island-dense regions on *GPX4* promoters were predicted using the UCSC Genome database (http://genome.ucsc.edu/). To improve the success rate of methylation-specific PCR, the *GPX4* promoter was divided into four fragments, with the primer sequences shown in Supplementary Table 4. DNA was extracted from liver tissues as previously described.[43] Unmethylated cytosine in the DNA was converted to uracil using the DNA Methylation-Gold kit.[44] The bisulfite-modified DNA was then used as a template for Sanger sequencing, amplified using the methylation-specific PCR kit. The sequencing results were analyzed using BioEditor software 7.0, which labeled the corresponding cytosine peaks at the CpG site and the thymine peaks. The Beta-value was calculated according to the following formula:

$$\text{Beta-value} = \frac{\text{C-reads}}{\text{C-reads} + \text{T-reads}}$$

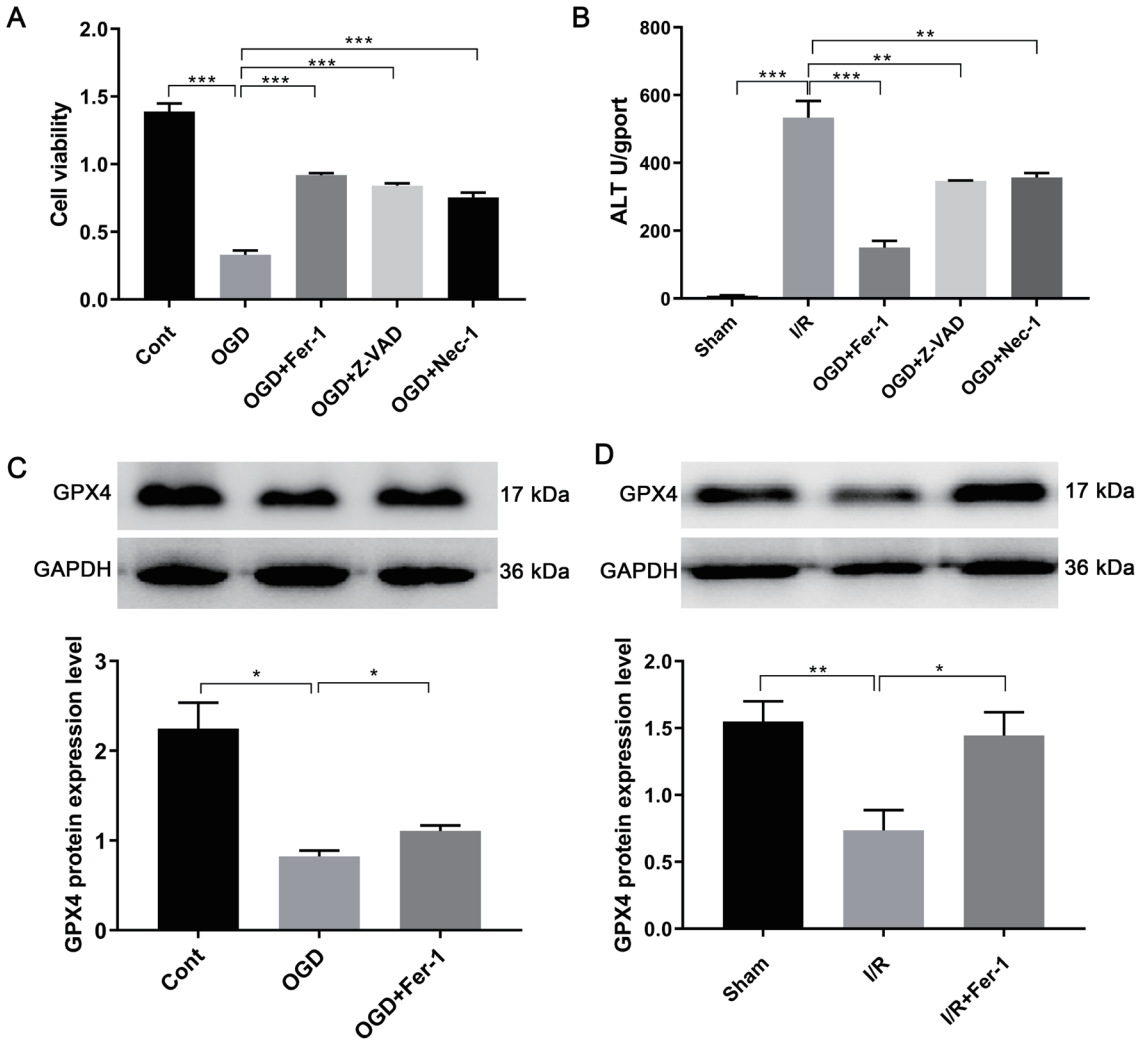

Fig. 1. Ferroptosis-related changes after hepatic ischemia-reperfusion injury (HIRI). (A) Cell viability after oxygen and glucose deprivation (OGD) induction and the therapeutic effects of several different types of inhibitors: ferroptosis inhibitor Fer-1, apoptosis inhibitor Z-VAD, and necrosis inhibitor Nec-1. (B) Alanine aminotransferase levels after I/R induction and the therapeutic effects of Fer-1, Z-VAD, and Nec-1 *in vivo*. Protein expression levels of GPX4 after HIRI and the therapeutic effect of Fer-1 *in vitro* (C) and *in vivo* (D). *$p < 0.05$, **$p < 0.01$, ***$p < 0.001$. Cont, the control group; ALT, alanine aminotransferase; GAPDH, glyceraldehyde-3-phosphate dehydrogenase.

Detection of 5mC and 5hmC

Methylation and hydroxymethylation of DNA were detected using ELISA kits as described in previous studies.[45] The DNA samples extracted from liver tissues were incubated with a chromogenic agent at room temperature for 3 m, and the absorbance was measured at 450 nm using a microplate reader.

Statistical analysis

SPSS 25.0 software was used for data analysis, and figures were created using GraphPad Prism 7 (GraphPad Software, Inc.). Data were collected from at least three independent experiments and expressed as mean ± standard error. The normality of distribution and homogeneity of variance were assessed using the Kolmogorov-SmI/Rnov test and the Levene test.[35] Comparisons among multiple groups were performed using a one-way analysis of variance followed by the least significant difference test. Data that were not normally distributed were analyzed using Kruskal-Wallis nonparametric tests, followed by Bonferroni post hoc tests for comparison. A *P*-value of less than 0.05 was considered statistically significant.

Results

Ferroptosis was the major type of cellular death after OGD or I/R induction

The CCK8 assay showed that the cell viability of AML12 cells decreased after OGD induction compared to the control group (0.33 ± 0.01 vs. 1.39 ± 0.02, $P < 0.05$). However, pretreatment with Fer-1, Z-VAD, or Nec-1 reversed the changes induced by OGD (Fig. 1A), with Fer-1 showing the most significant effect on the recovery of cell activity (0.92 ± 0.01 vs. 0.33 ± 0.01, $P < 0.01$). *In vivo* experiments also confirmed that Fer-1 antagonized the increased serum ALT levels induced by I/R (305.1 ± 25.3 vs. 208.7 ± 14.1, $P < 0.05$, Fig. 1B).

The expression of GPX4 was significantly downregulated in the OGD group compared to the control group (Fig. 1C and D).

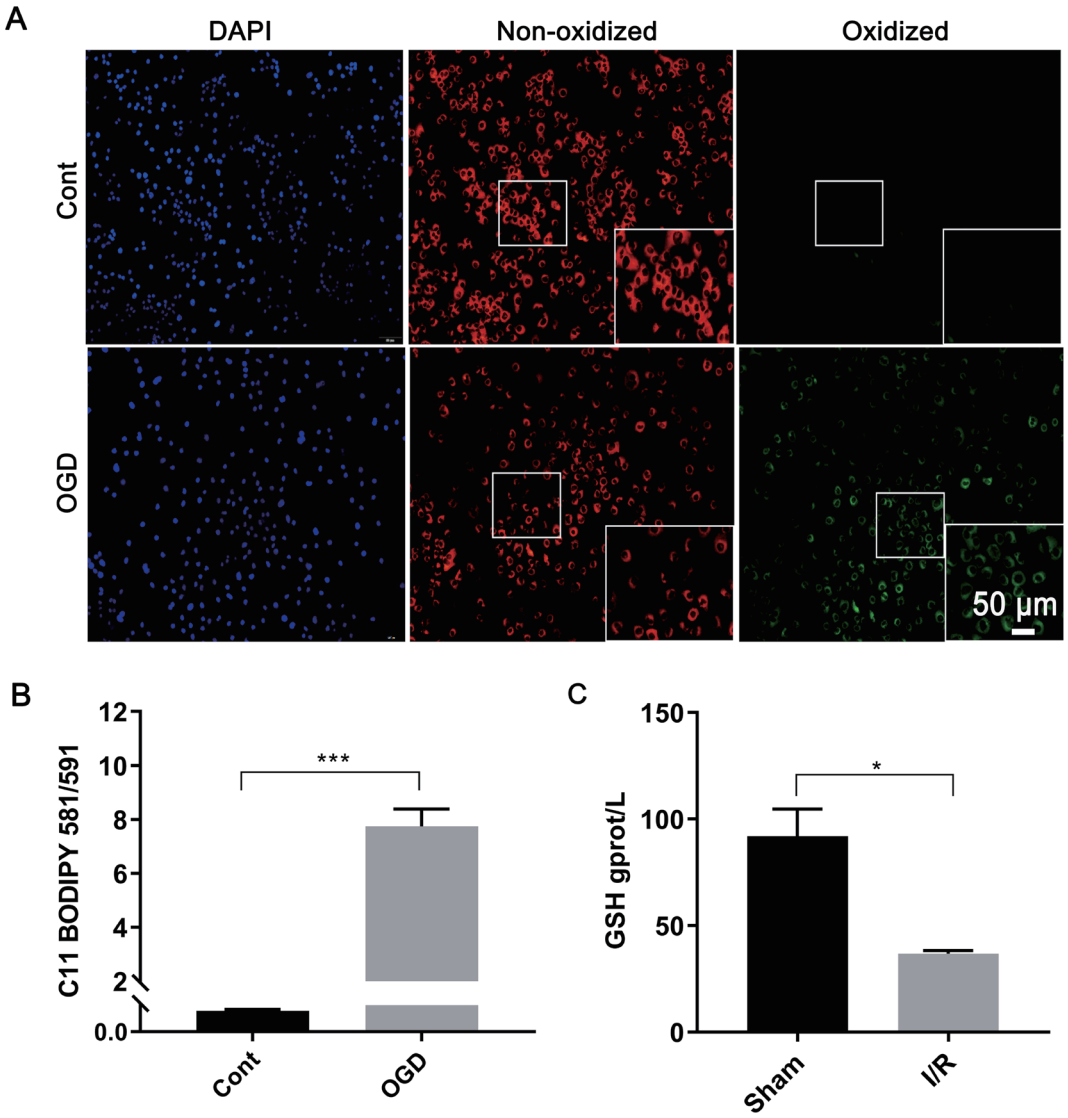

Fig. 2. Lipid peroxide levels after hepatic ischemia-reperfusion injury. (A) Fluorescence staining images (20×) and (B) microplate reader results for cell models stained with C11 BODIPY 581/591 in the Cont and OGD groups. (C) Glutathione (GSH) levels. *p < 0.05, ***p < 0.001. Cont, the control; DAPI, 4′,6-diamidino-2-phenylindole; OGD, oxygen and glucose deprivation cell model.

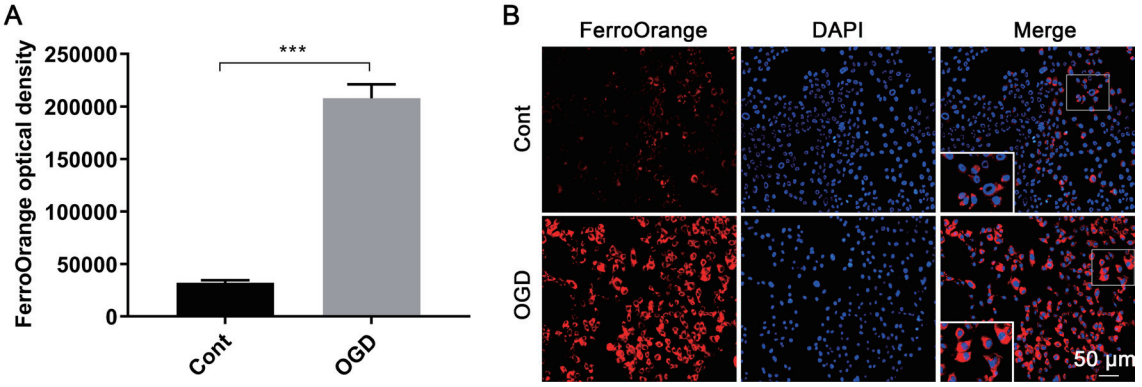

Fig. 3. Ferrous ion levels after OGD induction. (A) Results from the microplate reader and (B) fluorescence staining images (20×) stained with FerroOrange. ***p < 0.001. Cont, the control group; OGD, oxygen and glucose deprivation cell model; DAPI, 4′,6-diamidino-2-phenylindole.

This downregulation was significantly reversed in the presence of Fer-1 (0.76 ± 0.06 vs. 0.92 ± 0.35, $P < 0.05$, Fig. 1C). *In vivo* data confirmed that Fer-1 almost completely restored the I/R-induced downregulation of GPX4 (0.74 ± 0.15 vs. 1.44 ± 0.17, $P < 0.05$, Fig. 1D). These results suggest that ferroptosis was the major form of hepatocyte death following I/R.

The level of lipid peroxidation and ferrous ions was increased

Fluorescence microscopy revealed that DAPI staining indicated an increased percentage of AML12 cell death after OGD induction. C11 BODIPY 581/591 staining showed a significant increase in green fluorescence, representing the oxidized form, and a decrease in red fluorescence, representing the reduced form (Fig. 2A). Furthermore, the ELISA assay showed that the OD510nm/OD591nm ratio was significantly higher in the OGD group compared to the control group (7.74 ± 0.64 vs. 0.065 ± 0.004, $P < 0.01$, Fig. 2B), indicating the accumulation of lipid peroxides in AML12 cells after OGD.

The GSH content in liver tissue showed a significant decrease in the I/R group compared to the sham group (36.80 ± 1.51 gprot/L vs. 91.99 ± 12.67 gprot/L, $P < 0.05$, Fig. 2C), indicating a loss of antioxidants in liver tissue after I/R. Collectively, these findings suggest that lipid peroxide accumulation was triggered following I/R.

After OGD induction, the fluorescence intensity of FerroOrange significantly increased compared to the control group (207,872 ± 3,182 vs. 31,971 ± 2,461, $P < 0.05$, Fig. 3A and B), demonstrating that the content of unstable Fe^{2+} was significantly elevated.

Altered expression of ferroptosis-related proteins

We examined the mRNA expression of *ACSL4*, *PTGS2*, and *GPX4* at 6 h, 12 h, and 24 h after reperfusion in the I/R model. The most significant changes in *ACSL4* expression were observed at 6 h, *PTGS2* at 12 h, and *GPX4* at 12 h (Supplementary Fig. 1). These time points were then selected to determine the effects of I/R induction on these three ferroptosis-related proteins.

The expression of *ACSL4* mRNA and protein was significantly higher in the I/R group compared to the sham group ($P < 0.05$, Fig. 4A). IF staining showed consistent results for protein expression after I/R.

Compared to the sham group, PTGS2 mRNA and protein expression were significantly upregulated in the I/R group ($P < 0.05$, Fig. 4B), and IF staining revealed similar upregulation of PTGS2.

GPX4 mRNA expression significantly decreased in the I/R group compared to the sham group (0.02 ± 0.01 vs. 0.13 ± 0.02, $P < 0.01$, Fig. 4C). Western blotting analysis also showed a significant decrease in GPX4 protein expression after I/R compared to the sham group (0.43 ± 0.06 vs. 0.87 ± 0.07, $P < 0.01$). IF results followed the same trend, suggesting reduced GPX4 expression during HIRI. ELISA results also confirmed a significant decrease in GPX4 activity after I/R (48.03 ± 2.86 vs. 60.26 ± 4.25, $P < 0.05$, Fig. 4C). These results indicate that changes in related proteins support the occurrence of ferroptosis following HIRI.

GPX4 was an important regulatory factor in ferroptosis

RT-qPCR and Western blotting analysis demonstrated that GPX4 was significantly knocked down after transfection ($P < 0.05$, Fig. 5A and B). OGD induced a significant decrease in cell viability compared with the control (0.70 ± 0.16 vs. 0.91 ± 0.02, $P < 0.01$, Fig. 5C), while GPX4 knockdown resulted in an even more pronounced reduction in activity (0.45 ± 0.01 vs. 0.91 ± 0.02, $P < 0.01$).C11 BODIPY 581/591 staining showed that knockdown of GPX4 further exacerbated OGD-induced lipid peroxidation (Fig. 5D). FerroOrange staining suggested that GPX4 knockdown also exacerbated OGD-induced intracellular iron overload (Fig. 5E).

To further explore the role of GPX4 in ferroptosis, GSH was added. GSH restored cell activity after OGD (1.069 ± 0.024 vs. 0.827 ± 0.027, $P < 0.05$, Fig. 5F). C11 BODIPY 591/581 staining indicated that GSH inhibited OGD-induced lipid peroxidation in AML12 cells (Fig. 5G), and FerroOrange staining revealed that exogenous GSH antagonized iron overload (Fig. 5H).

The methylation level of the GPX4 promoter was increased in HIRI

The UCSC database showed the presence of dense CpG islands in the promoter regions of *GPX4* (Fig. 6A), suggesting that *GPX4* expression may be regulated by methylation, potentially influencing HIRI-induced ferroptosis. RT-qPCR revealed that *GPX4* expression was significantly upregulated by 5-AZA compared with the control group (0.19 ± 0.01 vs. 0.11 ± 0.01, $P < 0.01$, Fig. 6B). Methylation-specific PCR and Sanger sequencing demonstrated an elevated methylation level of the *GPX4* promoter after HIRI (Fig. 6C).

The global methylation was increased in HIRI

To evaluate the activity of methyltransferases in HIRI, the mRNA expression of *DNMT1*, *DNMT3a*, and *DNMT3b* was first detected by RT-qPCR. DNMT3a exhibited the most significant change and was used as a marker for methylation (Fig. 7A, Supplementary Fig. 2A,B), with its expression level significantly higher compared to the sham group (0.003 ± 0.0005 vs. 0.001 ± 0.0003, $P < 0.05$). The protein expression was also significantly upregulated in the I/R group (1.85 ± 0.51 vs. 0.53 ± 0.05, $P < 0.05$), consistent with the IHC staining results.

RT-qPCR showed that TET1, TET2, and TET3 levels were significantly lower than those of the respective sham group (TET1: 0.00002 ± 0.0000003 vs. 0.00009 ± 0.00001; TET2: 0.01 ± 0.0000003 vs. 0.02 ± 0.004; TET3: 0.004 ± 0.0007 vs. 0.01 ± 0.002, $P < 0.01$, Supplementary Fig. 2). TET2 was more abundant than TET1 and TET3 in normal liver tissues, acting as a key factor representing DNA demethylation. Western blotting analysis showed that TET2 protein expression significantly decreased after I/R compared with the sham group (0.69 ± 0.12 vs. 1.65 ± 0.18, $P < 0.01$), consistent with the IHC results (Fig. 7B).

Additionally, the levels of 5mC and 5hmC were measured to reflect the degree of methylation and demethylation using the ELISA assay. Compared with the sham group, the 5mC level was significantly increased in the I/R group (1.08 ± 0.09 vs. 1.91 ± 0.17, $P < 0.05$), and the 5hmC content was decreased (0.001 ± 0.00008 vs. 0.001 ± 0.00001, $P < 0.05$, Fig. 7C), indicating an increase in global methylation following HIRI.

Discussion

In this study, we investigated changes in ferroptosis-related indicators and *GPX4* promoter methylation status during the pathogenesis of HIRI, using *in vivo* and *in vitro* models. We proposed that DNA methylation of the *GPX4* promoter may be involved in ferroptosis, playing an important role in the pathogenesis of HIRI.

Ferroptosis was first proposed by Scott J. Dixon *et al*. in 2012 and was distinguished from other modes of cell death by its unique characteristics. Morphologically, it is mainly charac-

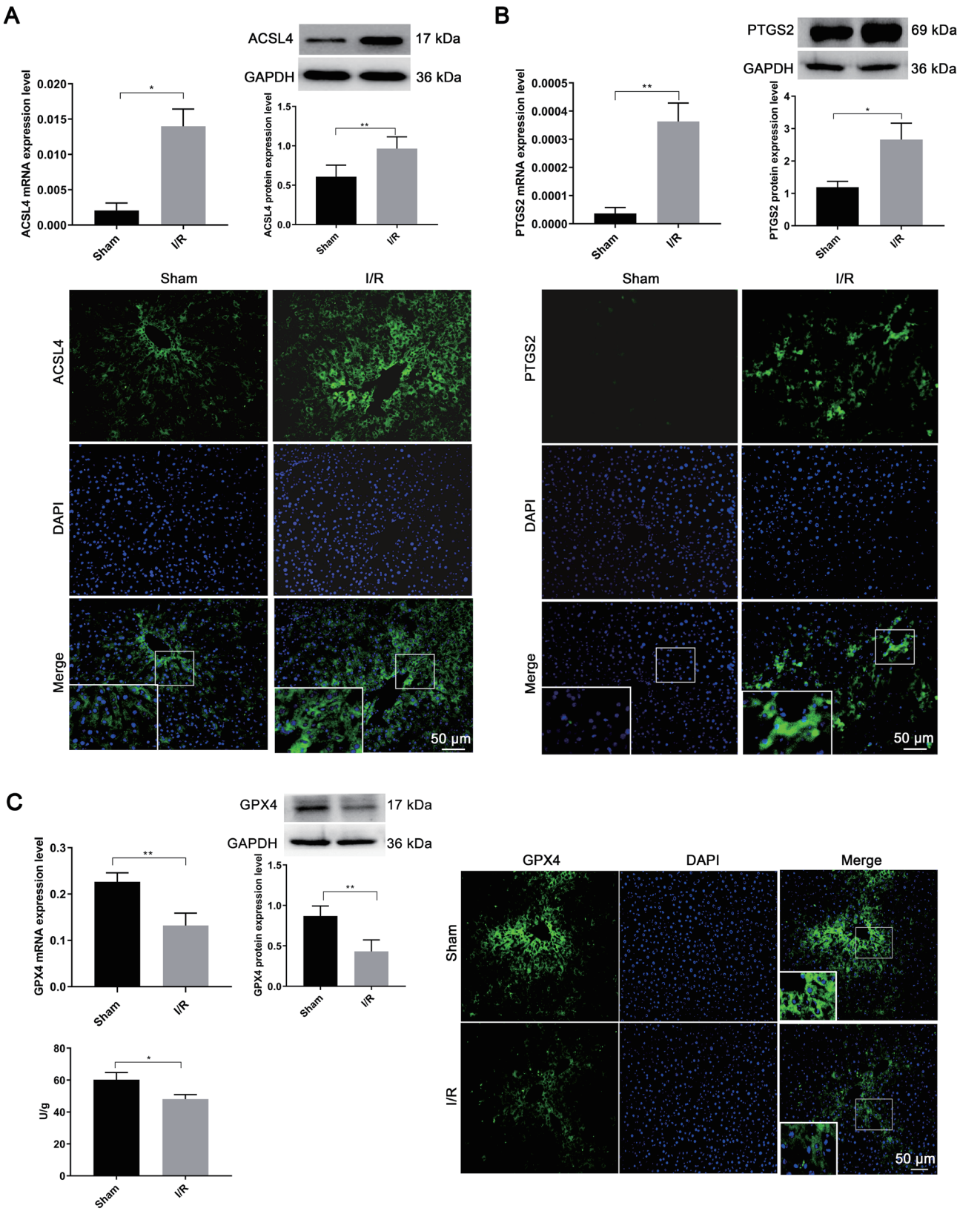

Fig. 4. Changes in ferroptosis-related proteins after hepatic ischemia-reperfusion injury. The mRNA and protein expression of (A) *ACSL4*, (B) *PTGS2,* (C) *GPX4*, and GPX4 enzyme activity. *$p < 0.05$, **$p < 0.01$. DAPI, 4′,6-diamidino-2-phenylindole; GAPDH, glyceraldehyde-3-phosphate dehydrogenase.

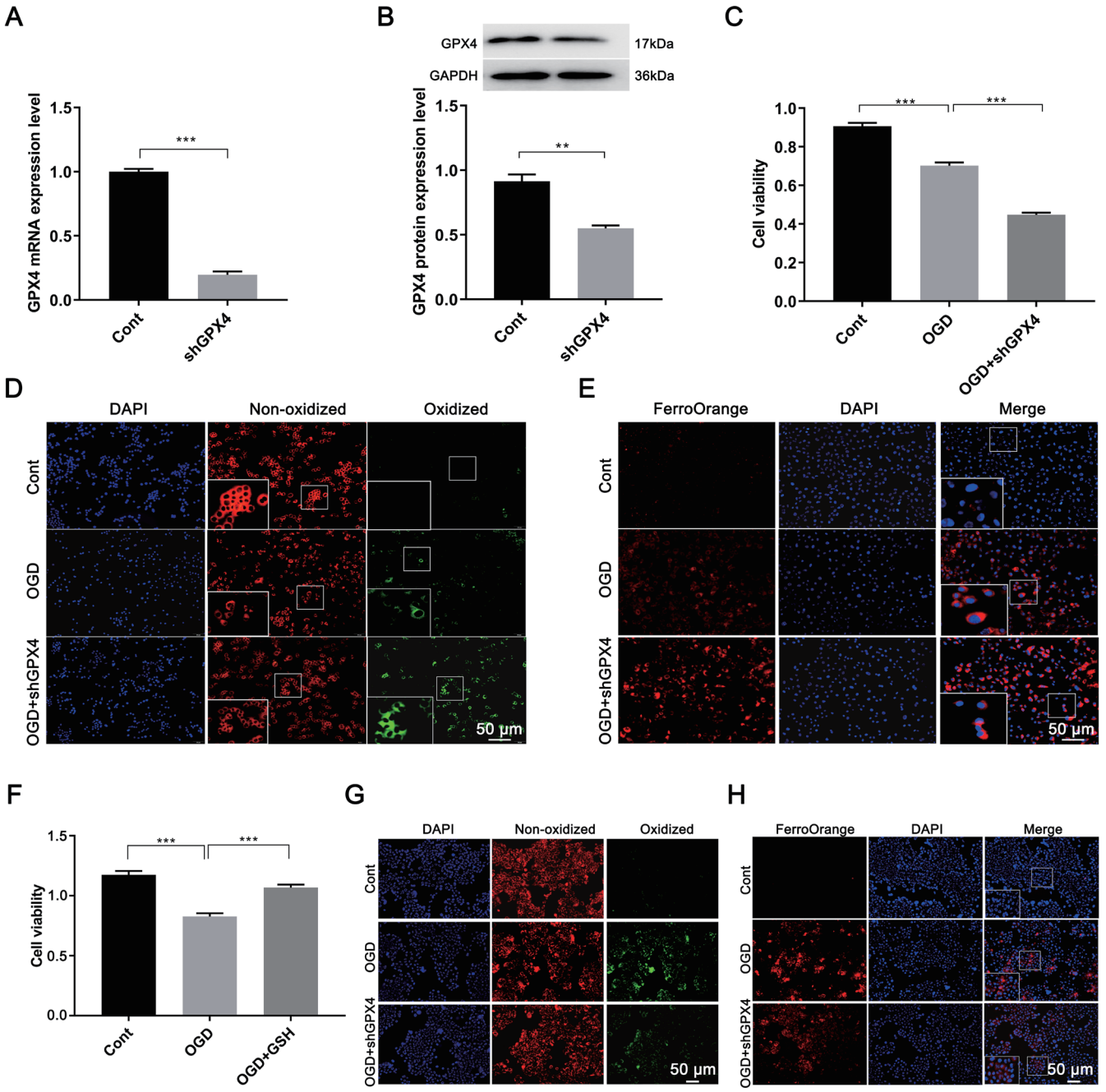

Fig. 5. *GPX4* expression and degree of ferroptosis after *GPX4* knockdown, and the therapeutic effect of glutathione. (A) mRNA and (B) protein expression of *GPX4*. (C) Cell viability. Fluorescent images (20×) stained with (D) C11 BODIPY 581/591 and (E) FerroOrange. The therapeutic effect of glutathione on ferroptosis was assessed by (F) cell viability, (G) the degree of lipid peroxidation, and (H) iron ion levels. $^{**}p < 0.01$, $^{***}p < 0.001$. Cont, the control group; DAPI, 4′,6-diamidino-2-phenylindole; OGD, the group of oxygen and glucose deprivation cell model.

terized by smaller cell size, mitochondrial shrinkage, greater membrane density, and the reduction or disappearance of mitochondrial cristae, with no obvious nuclear changes.[17] Biochemically, ferroptosis is marked by elevated ferrous ions and the accumulation of lipid peroxides. Subsequent studies showed that ferroptosis cannot be antagonized by specific inhibitors of necrosis, apoptosis, or autophagy.[46] However, it can be inhibited by iron chelators or antioxidants, indicating that ferroptosis is a distinct form of cell death.[47] In a previous study, Guo *et al*. reported that Fer-1 intervention attenuated I/R-induced cardiomyocyte dysfunction, which was accompanied by elevated Fe^{2+} and ROS and reduced GPX4.[48] In this study, different types of inhibitors were employed to restore cell viability, with the ferroptosis inhibitor Fer-1 showing the most significant effect. These results imply that ferroptosis may be the major form of cellular death in IRI.

There are many reports of ferroptosis-related studies on I/R in the heart, brain, or kidney, but fewer studies have fo-

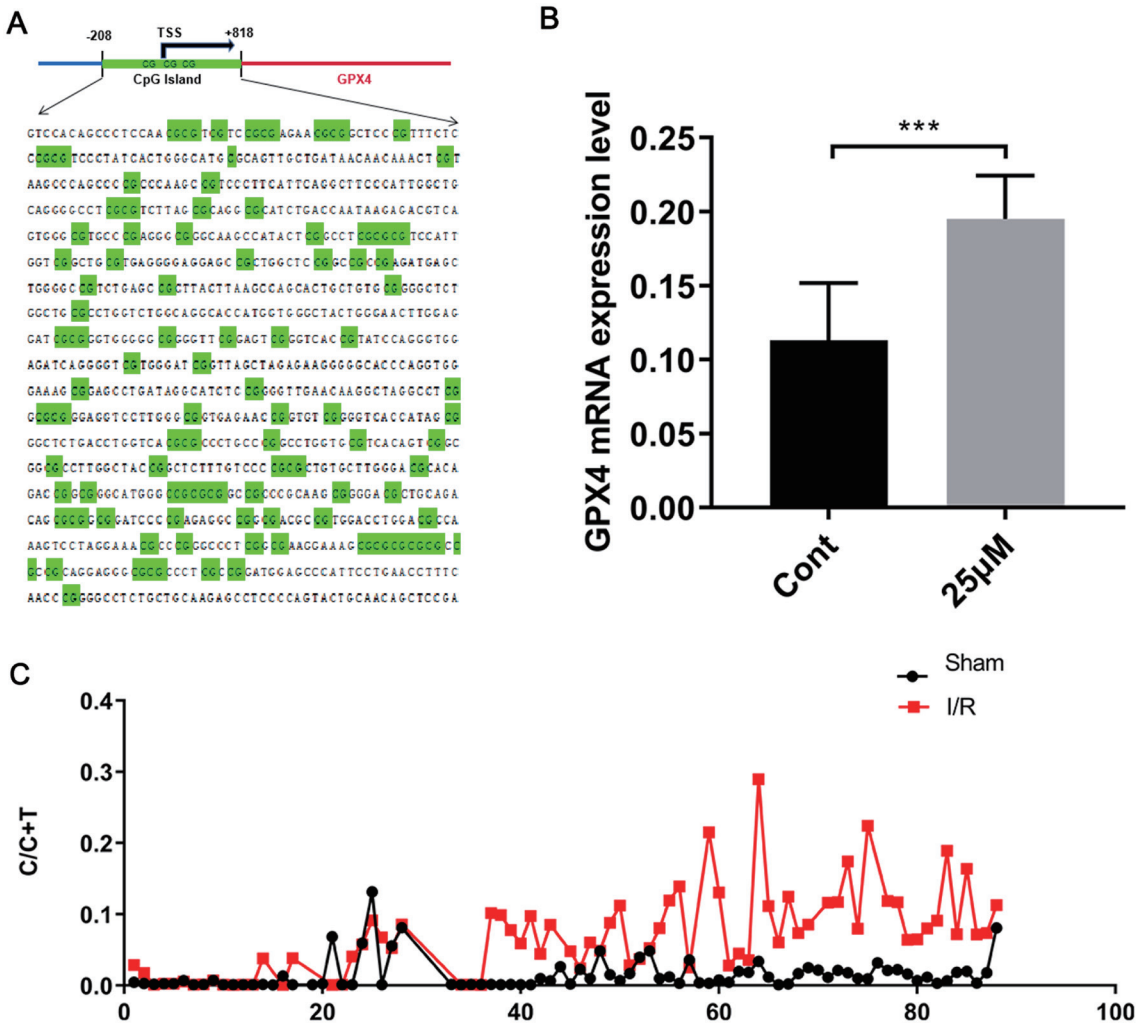

Fig. 6. Methylation level of the *GPX4* promoter after hepatic ischemia-reperfusion injury. (A) Dense distribution of CpG islands in the DNA promoter region of *GPX4*, identified by UCSC database analysis. (B) *GPX4* expression after pretreatment with the specific demethylating drug 5-AZA. (C) Methylation level of the *GPX4* promoter. ***$p < 0.001$. Cont, the control group.

cused on ferroptosis in HIRI. Naoya *et al*. analyzed perioperative data from 202 patients who underwent liver transplantation due to congenital biliary atresia and found that elevated serum ferritin was an independent risk factor for impaired hepatic function, indicating the occurrence of iron overload.[49] Some studies reported changes in ferroptosis after HIRI in mice, including elevated lipid peroxidation products and high expression of ferroptosis-associated proteins ACSL4 and PTGS2.[14] It was reported that some compounds can antagonize these changes, exerting protective effects on hepatocytes.[50–52] For example, the ferroptosis inhibitor liproxstatin-1 attenuated HIRI by inhibiting lipid peroxidation.[4,53] Naringenin can downregulate total iron content and Fe^{2+} levels, inhibit lipid peroxidation and the expression of ferroptosis-associated proteins, and attenuate IRI.[54] Curcumin and Lox-Block-1 reduced ACSL4 levels in liver and pancreas tissues, thereby inhibiting lipid peroxidation and iron-induced damage through their antioxidant properties after reperfusion.[55] This study revealed increased lipid peroxidation and iron ion levels following HIRI, accompanied by elevated expression of ferroptosis-related proteins (i.e., ACSL4 and PTGS2).

As an important antioxidant, GPX4 plays a role in maintaining cellular function by reducing toxic lipid peroxides to lipid alcohols.[56] Its downregulation is a critical event in ferroptosis. Knockdown or inhibition of *GPX4* has been shown to lead to the accumulation of lipid peroxides and the formation of lipid free radicals catalyzed by intracellular iron ions, thereby increasing cellular susceptibility to ferroptosis.[57] For example, Zhang *et al*. showed that *GPX4* knockdown exacerbated brain injury after cerebral hemorrhage using specific inhibitors or siRNA.[58] Similarly, in this study, *GPX4* mRNA and protein expression levels were significantly reduced after HIRI. Knockdown of *GPX4* exacerbated OGD-induced cell injury, characterized by a more pronounced decrease in cellular activity, accumulation of intracellular lipid peroxides, and increased staining for ferrous ions. Moreover, GSH could attenuate these changes, providing a protective effect against HIRI. All these results support that GPX4 is a key regulator of ferroptosis.

The expression of *GPX4* is influenced by various epigenetic regulators, such as DNA methylation. Studies have shown that methylation of the *GPX4* promoter can downregulate its expression, reducing cellular antioxidant capacity, leading to the accumulation of lipid peroxides, and ultimately causing

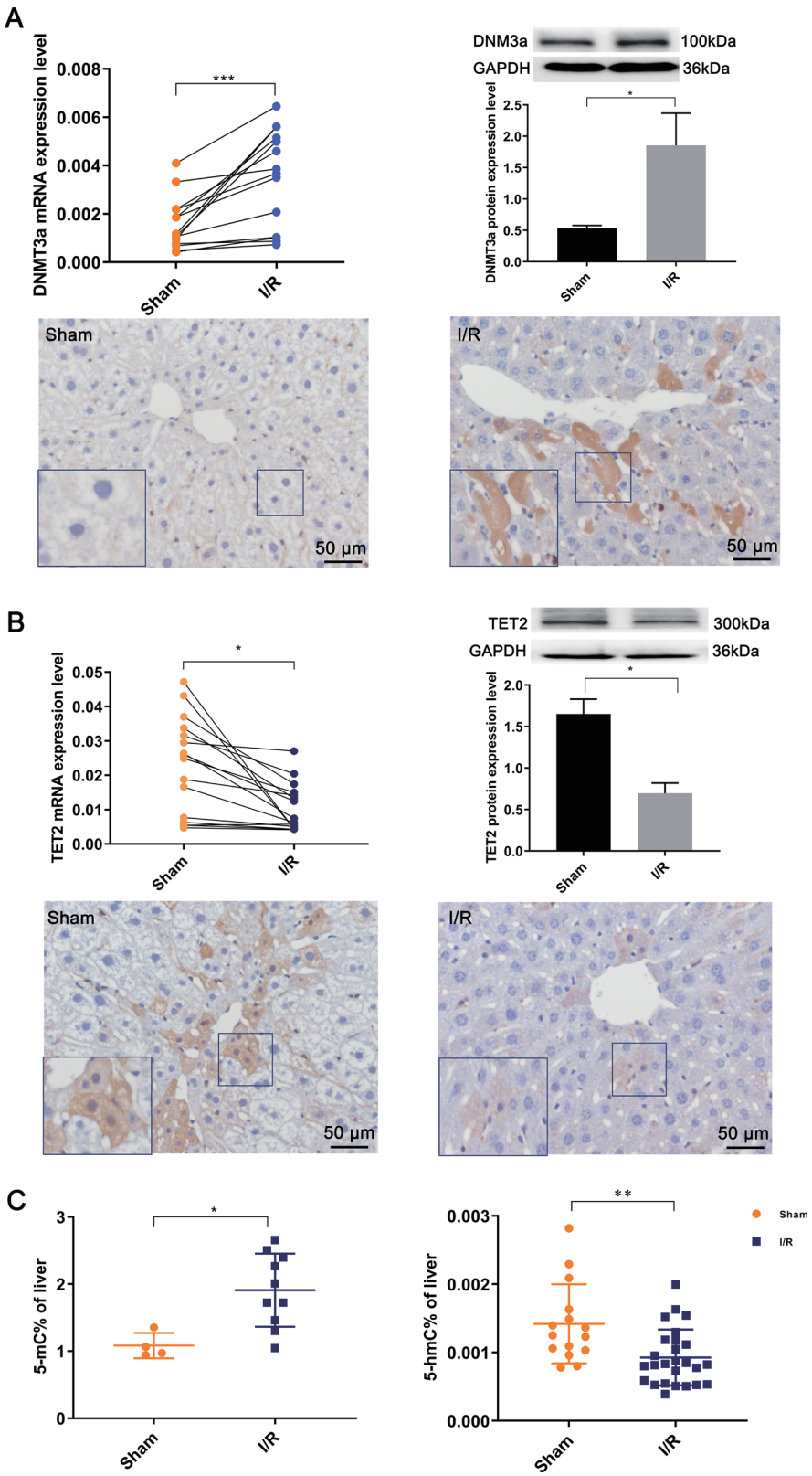

Fig. 7. Global methylation levels after hepatic ischemia-reperfusion injury. The mRNA and protein expression of (A) *DNMT3a* and (B) *TET2*, along with respective IHC (200×) results. (C) ELISA results showed DNA levels of 5mC and 5hmC. *$p < 0.05$, **$p < 0.01$, ***$p < 0.001$. GAPDH, glyceraldehyde-3-phosphate dehydrogenase; *TET2*, ten-eleven- translocation family 2; *DNMT3a*, DNA methyltransferase 3 alpha.

ferroptosis.[59,60] For example, Liu *et al*. found that Ubiquitin-like with PHD and RING Finger domains 1 promoted the methylation of the *GPX4* promoter, inhibiting its expression and accelerating ferroptosis in alveolar epithelial Type 2 cells.[59] A similar study proposed that methylation of the *GPX4* promoter could reduce the GPX4 expression and enhance ferroptosis sensitivity in fibroblast-like synoviocytes.[61] DNA methylation generally occurs at the CpG sites. Pratt *et al*. first reported altered DNA methylation in renal IRI, finding that the promoter region of the complement factor C3 gene showed aberrant DNA methylation and downregulation of overall 5hmC levels in a rat renal I/R model.[62] The mRNA expression of *TET1* and *TET2* was significantly decreased in kidney tissues after I/R.[63] Endres *et al*. also demonstrated that overall DNA methylation was upregulated in the brain following mild focal cerebral ischemia, and IRI led to a triple to quadruple increase in methyl binding.[64] Nevertheless, the methylation-specific inhibitor 5-AZA ameliorated ischemic brain injury and reduced cerebral infarct areas, suggesting that methylation status could affect cerebral I/R-induced cellular damage.[65,66] The roles of methylation have also been confirmed in myocardial I/R. For instance, Li *et al.* reported altered methylation levels of all 47 CpGs based on genome-wide DNA methylation assays in human acute myocardial infarction cases.[57] As a specific methylase inhibitor, 5-AZA was able to reverse nicotine-induced left ventricular dysfunction and reduce the incidence of myocardial infarction in offspring rats.[67] In our study, the global methylation increased following IRI. UCSC analysis showed that CpG islands were abundant in the *GPX4* promoter region, where sequencing revealed that IRI increased methylation, while *GPX4* expression was upregulated in the presence of 5-AZA. Our findings collectively demonstrate that IRI affects the methylation of the GPX4 promoter.

However, there are some limitations in this study. For example, we failed to explore whether changes in methylase expression can affect the HIRI degree. Nevertheless, this study provides new evidence and a foundation for understanding the mechanisms of hepatic I/R injury, which may be conducive to future research on new targets and therapeutic approaches.

Conclusions

We explored the role of ferroptosis in the pathogenesis of HIRI. We found increased methylation of the *GPX4* promoter and decreased *GPX4* expression, accompanied by elevated levels of 5mC and DNMTs, and decreased levels of 5hmC and TETs. Our study demonstrated that ferroptosis is associated with *GPX4* promoter methylation and global methylation following HIRI.

Funding

This work was supported by the Natural Science Foundation of Shandong Province (No. ZR2022MH011, No. ZR202111200086) and the Medical and Health Science and Technology Development Project of Shandong Province (No. 202001020642).

Conflict of interest

The authors have no conflicts of interest related to this publication.

Author contributions

Research conception and design (JL, JJ, SY), experiment performance (CB, YC, FC), data analysis (PX, FC, YJ, JF, YZ, JL), experiment result interpretation (CB, PX, YC), figure preparation (CB, PX, YC), manuscript drafting (CB, PX, YC), manuscript editing and revision (JJ, JL, SY). All authors have approved the final version and publication of the manuscript.

Ethical statement

All procedures were conducted in accordance with the guidelines of the animal ethics committee of Shandong Second Medical University Medical Ethics Committee, which provided full approval for this research (Approval No. 2020SDL187). All animals received human care.

Data sharing statement

All data generated or analyzed during this study are included in this published article and its supplementary information files.

References

[1] Saidi RF, Kenari SK. Liver ischemia/reperfusion injury: an overview. J Invest Surg 2014;27(6):366–379. doi:10.3109/08941939.2014.932473, PMID:25058854.
[2] van Golen RF, Reiniers MJ, Olthof PB, van Gulik TM, Heger M. Sterile inflammation in hepatic ischemia/reperfusion injury: present concepts and potential therapeutics. J Gastroenterol Hepatol 2013;28(3):394–400. doi:10.1111/jgh.12072, PMID:23216461.
[3] Kerins MJ, Ooi A. The Roles of NRF2 in Modulating Cellular Iron Homeostasis. Antioxid Redox Signal 2018;29(17):1756–1773. doi:10.1089/ars.2017.7176, PMID:28793787.
[4] Macías-Rodríguez RU, Inzaugarat ME, Ruiz-Margáin A, Nelson LJ, Trautwein C, Cubero FJ. Reclassifying Hepatic Cell Death during Liver Damage: Ferroptosis-A Novel Form of Non-Apoptotic Cell Death? Int J Mol Sci 2020;21(5):1651. doi:10.3390/ijms21051651, PMID:32121273.
[5] Yamada N, Karasawa T, Wakiya T, Sadatomo A, Ito H, Kamata R, *et al*. Iron overload as a risk factor for hepatic ischemia-reperfusion injury in liver transplantation: Potential role of ferroptosis. Am J Transplant 2020;20(6):1606–1618. doi:10.1111/ajt.15773, PMID:31909544.
[6] Tao WH, Shan XS, Zhang JX, Liu HY, Wang BY, Wei X, *et al*. Dexmedetomidine Attenuates Ferroptosis-Mediated Renal Ischemia/Reperfusion Injury and Inflammation by Inhibiting ACSL4 via α2-AR. Front Pharmacol 2022;13:782466. doi:10.3389/fphar.2022.782466, PMID:35873574.
[7] Bayır H, Anthonymuthu TS, Tyurina YY, Patel SJ, Amoscato AA, Lamade AM, *et al*. Achieving Life through Death: Redox Biology of Lipid Peroxidation in Ferroptosis. Cell Chem Biol 2020;27(4):387–408. doi:10.1016/j.chembiol.2020.03.014, PMID:32275865.
[8] Cui J, Wang Y, Tian X, Miao Y, Ma L, Zhang C, *et al*. LPCAT3 Is Transcriptionally Regulated by YAP/ZEB/EP300 and Collaborates with ACSL4 and YAP to Determine Ferroptosis Sensitivity. Antioxid Redox Signal 2023;39(7-9):491–511. doi:10.1089/ars.2023.0237, PMID:37166352.
[9] Yuan H, Li X, Zhang X, Kang R, Tang D. Identification of ACSL4 as a biomarker and contributor of ferroptosis. Biochem Biophys Res Commun 2016;478(3):1338–1343. doi:10.1016/j.bbrc.2016.08.124, PMID:27565726.
[10] Han L, Ma C, Wu Z, Xu H, Li H, Pan G. AhR-STAT3-HO-1/COX-2 signalling pathway may restrict ferroptosis and improve hMSC accumulation and efficacy in mouse liver. Br J Pharmacol 2024;181(1):125–141. doi:10.1111/bph.16208, PMID:37538043.
[11] Chai JL, Lu BW, Du HT, Wen MT, Liang XZ, Wang P. Pyroptosis -related potential diagnostic biomarkers in steroid-induced osteonecrosis of the femoral head. BMC Musculoskelet Disord 2023;24(1):609. doi:10.1186/s12891-023-06729-8, PMID:37491198.
[12] Yang WS, SriRamaratnam R, Welsch ME, Shimada K, Skouta R, Viswanathan VS, *et al*. Regulation of ferroptotic cancer cell death by GPX4. Cell 2014;156(1-2):317–331. doi:10.1016/j.cell.2013.12.010, PMID:24439385.
[13] Zhou Y, Zhou H, Hua L, Hou C, Jia Q, Chen J, *et al*. Verification of ferroptosis and pyroptosis and identification of PTGS2 as the hub gene in human coronary artery atherosclerosis. Free Radic Biol Med 2021;171:55–68. doi:10.1016/j.freeradbiomed.2021.05.009, PMID:33974977.
[14] Han L, Ma C, Wu Z, Xu H, Li H, Pan G. AhR-STAT3-HO-1/COX-2 signalling pathway may restrict ferroptosis and improve hMSC accumulation and efficacy in mouse liver. Br J Pharmacol 2024;181(1):125–141. doi:10.1111/bph.16208, PMID:37538043.
[15] Zhang Y, Swanda RV, Nie L, Liu X, Wang C, Lee H, *et al*. mTORC1 couples cyst(e)ine availability with GPX4 protein synthesis and ferroptosis regulation. Nat Commun 2021;12(1):1589. doi:10.1038/s41467-021-21841-w, PMID:33707434.
[16] Yang W, Wang Y, Zhang C, Huang Y, Yu J, Shi L, *et al*. Maresin1 Protect Against Ferroptosis-Induced Liver Injury Through ROS Inhibition and Nrf2/HO-1/GPX4 Activation. Front Pharmacol 2022;13:865689. doi:10.3389/

fphar.2022.865689, PMID:35444546.
[17] Dixon SJ, Lemberg KM, Lamprecht MR, Skouta R, Zaitsev EM, Gleason CE, *et al*. Ferroptosis: an iron-dependent form of nonapoptotic cell death. Cell 2012;149(5):1060–1072. doi:10.1016/j.cell.2012.03.042, PMID:22632970.
[18] Le NT, Richardson DR. Ferroportin1: a new iron export molecule? Int J Biochem Cell Biol 2002;34(2):103–108. doi:10.1016/s1357-2725(01)00104-2, PMID:11809412.
[19] Frey PA, Reed GH. The ubiquity of iron. ACS Chem Biol 2012;7(9):1477–1481. doi:10.1021/cb300323q, PMID:22845493.
[20] Wu Y, Zhang S, Gong X, Tam S, Xiao D, Liu S, *et al*. The epigenetic regulators and metabolic changes in ferroptosis-associated cancer progression. Mol Cancer 2020;19(1):39. doi:10.1186/s12943-020-01157-x, PMID:32103754.
[21] Wang Y, Liu T, Xu D, Shi H, Zhang C, Mo YY, *et al*. Predicting DNA Methylation State of CpG Dinucleotide Using Genome Topological Features and Deep Networks. Sci Rep 2016;6:19598. doi:10.1038/srep19598, PMID:26797014.
[22] Mudersbach T, Siuda D, Kohlstedt K, Fleming I. Epigenetic control of the angiotensin-converting enzyme in endothelial cells during inflammation. PLoS One 2019;14(5):e0216218. doi:10.1371/journal.pone.0216218, PMID:31042763.
[23] Jin B, Robertson KD. DNA methyltransferases, DNA damage repair, and cancer. Adv Exp Med Biol 2013;754:3–29. doi:10.1007/978-1-4419-9967-2_1, PMID:22956494.
[24] Zhang X, Zhang Y, Wang C, Wang X. TET (Ten-eleven translocation) family proteins: structure, biological functions and applications. Signal Transduct Target Ther 2023;8(1):297. doi:10.1038/s41392-023-01537-x, PMID:37563110.
[25] Song X, Long D. Nrf2 and Ferroptosis: A New Research Direction for Neurodegenerative Diseases. Front Neurosci 2020;14:267. doi:10.3389/fnins.2020.00267, PMID:32372896.
[26] Boovarahan SR, Kurian GA. Investigating the role of DNMT1 gene expression on myocardial ischemia reperfusion injury in rat and associated changes in mitochondria. Biochim Biophys Acta Bioenerg 2022;1863(6):148566. doi:10.1016/j.bbabio.2022.148566, PMID:35489443.
[27] Lv Y, Zhang C, Jian H, Lou Y, Kang Y, Deng W, *et al*. Regulating DNA methylation could reduce neuronal ischemia response and apoptosis after ischemia-reperfusion injury. Gene 2022;837:146689. doi:10.1016/j.gene.2022.146689, PMID:35750086.
[28] Jiang H, Fang Y, Wang Y, Li T, Lin H, Lin J, *et al*. FGF4 improves hepatocytes ferroptosis in autoimmune hepatitis mice via activation of CISD3. Int Immunopharmacol 2023;116:109762. doi:10.1016/j.intimp.2023.109762, PMID:36702076.
[29] Guerrero-Hue M, García-Caballero C, Palomino-Antolín A, Rubio-Navarro A, Vázquez-Carballo C, Herencia C, *et al*. Curcumin reduces renal damage associated with rhabdomyolysis by decreasing ferroptosis-mediated cell death. FASEB J 2019;33(8):8961–8975. doi:10.1096/fj.201900077R, PMID:31034781.
[30] Davies CW, Chaney J, Korbel G, Ringe D, Petsko GA, Ploegh H, *et al*. The co-crystal structure of ubiquitin carboxy-terminal hydrolase L1 (UCHL1) with a tripeptide fluoromethyl ketone (Z-VAE(OMe)-FMK). Bioorg Med Chem Lett 2012;22(12):3900–3904. doi:10.1016/j.bmcl.2012.04.124, PMID:22617491.
[31] Degterev A, Huang Z, Boyce M, Li Y, Jagtap P, Mizushima N, *et al*. Chemical inhibitor of nonapoptotic cell death with therapeutic potential for ischemic brain injury. Nat Chem Biol 2005;1(2):112–119. doi:10.1038/nchembio711, PMID:16408008.
[32] Zhou Y, Fan X, Jiao T, Li W, Chen P, Jiang Y, *et al*. SIRT6 as a key event linking P53 and NRF2 counteracts APAP-induced hepatotoxicity through inhibiting oxidative stress and promoting hepatocyte proliferation. Acta Pharm Sin B 2021;11(1):89–99. doi:10.1016/j.apsb.2020.06.016, PMID:33532182.
[33] Li W, Jiang H, Bai C, Yu S, Pan Y, Wang C, *et al*. Ac2-26 attenuates hepatic ischemia-reperfusion injury in mice via regulating IL-22/IL-22R1/STAT3 signaling. PeerJ 2022;10:e14086. doi:10.7717/peerj.14086, PMID:36193422.
[34] Cannistrà M, Ruggiero M, Zullo A, Gallelli G, Serafini S, Maria M, *et al*. Hepatic ischemia reperfusion injury: A systematic review of literature and the role of current drugs and biomarkers. Int J Surg 2016;33(Suppl 1):S57–S70. doi:10.1016/j.ijsu.2016.05.050, PMID:27255130.
[35] Bai C, Jiang Z, Jiang H, Yu S, Li M, Chu F, *et al*. Ac2-26 alleviates hepatic ischemia-reperfusion injury based on inhibiting the positive feedback loop of HMGB1/TLR4/NF-κB/neutrophils. Exp Ther Med 2022;24(5):673. doi:10.3892/etm.2022.11609, PMID:36237600.
[36] Du S, Zhang X, Jia Y, Peng P, Kong Q, Jiang S, *et al*. Hepatocyte HSPA12A inhibits macrophage chemotaxis and activation to attenuate liver ischemia/reperfusion injury via suppressing glycolysis-mediated HMGB1 lactylation and secretion of hepatocytes. Theranostics 2023;13(11):3856–3871. doi:10.7150/thno.82607, PMID:37441587.
[37] Reduced glutathione (GSH) assay kit. Available from: http://www.njjcbio.com/uploadfile/product/big/20240712111029965.pdf.
[38] Drummen GP, van Liebergen LC, Op den Kamp JA, Post JA. C11-BODIPY(581/591), an oxidation-sensitive fluorescent lipid peroxidation probe: (micro)spectroscopic characterization and validation of methodology. Free Radic Biol Med 2002;33(4):473–490. doi:10.1016/s0891-5849(02)00848-1, PMID:12160930.
[39] Mei H, Zhao L, Li W, Zheng Z, Tang D, Lu X, *et al*. Inhibition of ferroptosis protects House Ear Institute-Organ of Corti 1 cells and cochlear hair cells from cisplatin-induced ototoxicity. J Cell Mol Med 2020;24(20):12065–12081. doi:10.1111/jcmm.15839, PMID:32929878.
[40] Hussaini HM, Seo B, Rich AM. Immunohistochemistry and Immunofluorescence. Methods Mol Biol 2023;2588:439–450. doi:10.1007/978-1-0716-2780-8_26, PMID:36418703.
[41] Ming He J, Liu PY, Wang J. MicroRNA-17-5p regulates the growth, migration and invasion of the human osteosarcoma cells by modulating the expression of PTEN. J BUON 2020;25(2):1028–1034. PMID:32521902.
[42] Livak KJ, Schmittgen TD. Analysis of relative gene expression data using real-time quantitative PCR and the 2(-Delta Delta C(T)) Method. Methods 2001;25(4):402–408. doi:10.1006/meth.2001.1262, PMID:11846609.
[43] He B, Zhang C, Zhang X, Fan Y, Zeng H, Liu J, *et al*. Tissue-specific 5-hydroxymethylcytosine landscape of the human genome. Nat Commun 2021;12(1):4249. doi:10.1038/s41467-021-24425-w, PMID:34253716.
[44] July J, Patricia D, Gunawan PY, Setiajaya H, Ginting TE, Putra TP, *et al*. Clinicopathological associations and prognostic values of IDH1 gene mutation, MGMT gene promoter methylation, and PD-L1 expressions in high-grade glioma treated with standard treatment. Pan Afr Med J 2020;36:309. doi:10.11604/pamj.2020.36.309.24831, PMID:33282092.
[45] Yamazaki M, Munetsuna E, Yamada H, Ando Y, Mizuno G, Murase Y, *et al*. Fructose consumption induces hypomethylation of hepatic mitochondrial DNA in rats. Life Sci 2016;149:146–152. doi:10.1016/j.lfs.2016.02.020, PMID:26869391.
[46] Yagoda N, von Rechenberg M, Zaganjor E, Bauer AJ, Yang WS, Fridman DJ, *et al*. RAS-RAF-MEK-dependent oxidative cell death involving voltage-dependent anion channels. Nature 2007;447(7146):864–868. doi:10.1038/nature05859, PMID:17568748.
[47] Egolf S, Zou J, Anderson A, Simpson CL, Aubert Y, Prouty S, *et al*. MLL4 mediates differentiation and tumor suppression through ferroptosis. Sci Adv 2021;7(50):eabj9141. doi:10.1126/sciadv.abj9141, PMID:34890228.
[48] Guo Y, Lu C, Hu K, Cai C, Wang W. Ferroptosis in Cardiovascular Diseases: Current Status, Challenges, and Future Perspectives. Biomolecules 2022;12(3):390. doi:10.3390/biom12030390, PMID:35327582.
[49] Yamada N, Karasawa T, Kimura H, Watanabe S, Komada T, Kamata R, *et al*. Ferroptosis driven by radical oxidation of n-6 polyunsaturated fatty acids mediates acetaminophen-induced acute liver failure. Cell Death Dis 2020;11(2):144. doi:10.1038/s41419-020-2334-2, PMID:32094346.
[50] Sun Y, Zheng Y, Wang C, Liu Y. Glutathione depletion induces ferroptosis, autophagy, and premature cell senescence in retinal pigment epithelial cells. Cell Death Dis 2018;9(7):753. doi:10.1038/s41419-018-0794-4, PMID:29988039.
[51] Liu H, Forouhar F, Seibt T, Saneto R, Wigby K, Friedman J, *et al*. Characterization of a patient-derived variant of GPX4 for precision therapy. Nat Chem Biol 2022;18(1):91–100. doi:10.1038/s41589-021-00915-2, PMID:34931062.
[52] Zhang Y, Liu Y, Liu X, Yuan X, Xiang M, Liu J, *et al*. Exercise and Metformin Intervention Prevents Lipotoxicity-Induced Hepatocyte Apoptosis by Alleviating Oxidative and ER Stress and Activating the AMPK/Nrf2/HO-1 Signaling Pathway in db/db Mice. Oxid Med Cell Longev 2022;2022:2297268. doi:10.1155/2022/2297268, PMID:36120597.
[53] Friedmann Angeli JP, Schneider M, Proneth B, Tyurina YY, Tyurin VA, Hammond VJ, *et al*. Inactivation of the ferroptosis regulator Gpx4 triggers acute renal failure in mice. Nat Cell Biol 2014;16(12):1180–1191. doi:10.1038/ncb3064, PMID:25402683.
[54] Xu S, Wu B, Zhong B, Lin L, Ding Y, Jin X, *et al*. Naringenin alleviates myocardial ischemia/reperfusion injury by regulating the nuclear factor-erythroid factor 2-related factor 2 (Nrf2) /System xc-/ glutathione peroxidase 4 (GPX4) axis to inhibit ferroptosis. Bioengineered 2021;12(2):10924–10934. doi:10.1080/21655979.2021.1995994, PMID:34699317.
[55] Kar F, Yıldız F, Hacioglu C, Kar E, Donmez DB, Senturk H, *et al*. LoxBlock-1 or Curcumin attenuates liver, pancreas and cardiac ferroptosis, oxidative stress and injury in Ischemia/reperfusion-damaged rats by facilitating ACSL/GPx4 signaling. Tissue Cell 2023;82:102114. doi:10.1016/j.tice.2023.102114, PMID:37210761.
[56] Forcina GC, Dixon SJ. GPX4 at the Crossroads of Lipid Homeostasis and Ferroptosis. Proteomics 2019;19(18):e1800311. doi:10.1002/pmic.201800311, PMID:30888116.
[57] Gautheron J, Gores GJ, Rodrigues CMP. Lytic cell death in metabolic liver disease. J Hepatol 2020;73(2):394–408. doi:10.1016/j.jhep.2020.04.001, PMID:32298766.
[58] Zhang X, Huang Z, Xie Z, Chen Y, Zheng Z, Wei X, *et al*. Homocysteine induces oxidative stress and ferroptosis of nucleus pulposus via enhancing methylation of GPX4. Free Radic Biol Med 2020;160:552–565. doi:10.1016/j.freeradbiomed.2020.08.029, PMID:32896601.
[59] Liu Y, Cheng D, Wang Y, Xi S, Wang T, Sun W, *et al*. UHRF1-mediated ferroptosis promotes pulmonary fibrosis via epigenetic repression of GPX4 and FSP1 genes. Cell Death Dis 2022;13(12):1070. doi:10.1038/s41419-022-05515-z, PMID:36566325.
[60] Hao M, Jiang Y, Zhang Y, Yang X, Han J. Ferroptosis regulation by methylation in cancer. Biochim Biophys Acta Rev Cancer 2023;1878(6):188972. doi:10.1016/j.bbcan.2023.188972, PMID:37634887.
[61] Ling H, Li M, Yang C, Sun S, Zhang W, Zhao L, *et al*. Glycine increased ferroptosis via SAM-mediated GPX4 promoter methylation in rheumatoid arthritis. Rheumatology (Oxford) 2022;61(11):4521–4534. doi:10.1093/rheumatology/keac069, PMID:35136972.
[62] Pratt JR, Parker MD, Affleck LJ, Corps C, Hostert L, Michalak E, *et al*. Ischemic epigenetics and the transplanted kidney. Transplant Proc 2006;38(10):3344–3346. doi:10.1016/j.transproceed.2006.10.112, PMID:17175268.
[63] Huang N, Tan L, Xue Z, Cang J, Wang H. Reduction of DNA hydroxymethylation in the mouse kidney insulted by ischemia reperfusion. Biochem Biophys Res Commun 2012;422(4):697–702. doi:10.1016/j.bbrc.2012.05.061, PMID:22627137.
[64] Endres M, Meisel A, Biniszkiewicz D, Namura S, Prass K, Ruscher K, *et*

al. DNA methyltransferase contributes to delayed ischemic brain injury. J Neurosci 2000;20(9):3175–3181. doi:10.1523/JNEUROSCI.20-09-03175.2000, PMID:10777781.
[65] Park TJ, Park JH, Lee GS, Lee JY, Shin JH, Kim MW, *et al*. Quantitative proteomic analyses reveal that GPX4 downregulation during myocardial infarction contributes to ferroptosis in cardiomyocytes. Cell Death Dis 2019;10(11):835. doi:10.1038/s41419-019-2061-8, PMID:31685805.
[66] Zhang Z, Tang J, Song J, Xie M, Liu Y, Dong Z, *et al*. Elabela alleviates ferroptosis, myocardial remodeling, fibrosis and heart dysfunction in hypertensive mice by modulating the IL-6/STAT3/GPX4 signaling. Free Radic Biol Med 2022;181:130–142. doi:10.1016/j.freeradbiomed.2022.01.020, PMID:35122997.
[67] Ke J, Dong N, Wang L, Li Y, Dasgupta C, Zhang L, *et al*. Role of DNA methylation in perinatal nicotine-induced development of heart ischemia-sensitive phenotype in rat offspring. Oncotarget 2017;8(44):76865–76880. doi:10.18632/oncotarget.20172, PMID:29100355.